2014 NASA Heliophysics Summer School

DYNAMO LAB NOTES

Paul Charbonneau
Département de Physique
Université de Montréal

June 2014

Contents

Chapter 1

Kinematic axisymmetric dynamo models {chap:dynmod}

It's not whether a thing is hard to understand.
It's whether, once understood, it makes any sense.

Hans Zinsser
Rats, Lice and History (1934)

These Notes contain information pertaining to the Laboratory component of the Lectures on stellar dynamos at the 2014 NASA Heliophysics Summer School. The Lab itelf consists in exploring the behavior of various types of dynamos as defining parameters are varied, as a means of interpreting observations of magnetic activity in late-type stars.

The truly impatients can skip directly to §1.5 and get going, but I strongly recommend that the preceeding sections be read at least rapidly, so as to know a bit how the dynamo solutions you will be working with are designed, and what the parameters you will be playing with relate to.

References to your *Heliophysics* textbooks are in the form Volume.chapter.section, e.g., III.6.2.1 refers to section 2.1 in chapter 6 of the third volume. I have also included a few homework problems and a short general bibliography at the end of the document.

1.1 Model design {sec:design}

The starting point is the magnetohydrodynamical induction equation (see §I.3.2):

$$\boxed{\frac{\partial \mathbf{B}}{\partial t} = \nabla \times (\mathbf{u} \times \mathbf{B} - \eta \nabla \times \mathbf{B})} \, . \tag{1.1}$$ {eq:induction}

where $\mathbf{u}$ is the total flow and η [$\mathrm{m}^2\,\mathrm{s}^{-1}$] the magnetic diffusivity. In the SI system of units, the the magnetic field $\mathbf{B}$ is measured in tesla (T).

We restrict ourselves here to kinematic, axisymmetric (two-dimensional) mean-field-like models, in the sense that we will be setting and solving partial differential equations for poloidal and toroidal large-scale magnetic components in a meridional $[r, \theta]$ plane, and subsume the effects of small-scale fluid motions and magnetic fields into coefficients of these PDEs (see §III.6.1). Working in spherical polar coordinates (r, θ, ϕ), the (time-indendent) large-scale flow and (time-dependent) magnetic field are expressed as

$$\mathbf{u}(r,\theta) = \mathbf{u}_p(r,\theta) + \varpi \Omega(r,\theta) \hat{\mathbf{e}}_\phi \ , \tag{1.2}$$ {eq:axiu}

$$\mathbf{B}(r,\theta,t) = \nabla \times (A(r,\theta,t)\hat{\mathbf{e}}_\phi) + B(r,\theta,t)\hat{\mathbf{e}}_\phi \ . \tag{1.3}$$ {eq:axiB}

where B is the large-scale toroidal (zonally-oriented) component of the magnetic field, the toroidal vector potential A defines the poloidal field, Ω is the rotational angular velocity (rad s^{-1}), and $\mathbf{u}_p$ is a large-scale flow component contained in meridional planes $[r,\theta]$, like the poloidal magentic field. Upon substituting these expressions into eq. (1.1), the latter can be separated into two coupled partial differential equations for A and B (see §III.6.XXX ...and problem 1!):

{eq:cowa}
$$\frac{\partial A}{\partial t} = \underbrace{\eta\left(\nabla^2 - \frac{1}{\varpi^2}\right)A}_{\text{resistive decay}} - \underbrace{\frac{\mathbf{u}_p}{\varpi}\cdot\nabla(\varpi A)}_{\text{advection}} \qquad + \qquad \underbrace{S(B)}_{poloidal source} \quad , \tag{1.4}$$

{eq:cowb}
$$\frac{\partial B}{\partial t} = \underbrace{\eta\left(\nabla^2 - \frac{1}{\varpi^2}\right)B}_{\text{resistive decay}} + \underbrace{\frac{1}{\varpi}\frac{\partial(\varpi B)}{\partial r}\frac{\partial \eta}{\partial r}}_{\text{diamagnetic transport}} \underbrace{-\varpi\nabla\cdot\left(\frac{B}{\varpi}\mathbf{u}_p\right)}_{\text{advection}} + \underbrace{\varpi(\nabla\times(A\hat{\mathbf{e}}_\phi))\cdot\nabla\Omega}_{\text{shearing}} \ . \tag{1.5}$$

with $\varpi = r\sin\theta$ and we have already anticipated that the total magnetic diffusivity η will depend only on depth. The source term $S(B)$ in eq. (1.4), usually taken to depend on the toroidal field B, does *not* arise from the substitution of eqs. (1.2)–(1.3) into (1.1). Its *ad hoc* introduction in eq. (1.4) is however essential for sustained dynamo action, in order to bypass Cowling's theorem (see §I.3.3.8). Specific prescriptions for this source term are discussed further below in §1.2.5.

Numerical solutions to eqs. (1.4)—(1.5) are sought in a meridional $[r,\theta]$ quadrant, spanning

{eq:domain}
$$0.5 \le r/R \le 1 \ , \qquad 0 \le \theta \le \pi/2 \ , \tag{1.6}$$

where R is the star's radius. For solar-like dynamos, most of the action takes place in the convecting layers ($0.7 \le r/R \le 1$ for the sun), but the solution domain includes part of the underlying stably-stratified radiative core, as the latter can play a significant role in the storage and amplification of magnetic fields.

In the "exterior" $r > R$ there is only vacuum. Whatever solution we compute in $r < R$ must be matched to a current-free solution in $r > R$. For an axisymmetric magnetic field this translates into

{eq:J0a}
$$\left(\nabla^2 - \frac{1}{\varpi^2}\right)A(r,\theta,t) = 0 \ , \tag{1.7}$$

{eq:J0b}
$$B(r,\theta,t) = 0 \ . \tag{1.8}$$

Note in particular that the vector potential A must be continuous up to its first derivative normal to the surface, so that the magnetic field component tangential to the surface remains continuous across $r = R$. Regularity of the magnetic field on the symmetry axis ($\theta = 0$) requires that we set $B = 0$ there. Without any loss of generality, we can also set $A = 0$ on the axis.

The boundary condition imposed on the equatorial plane ($\theta = \pi/2$) sets the equatorial symmetry (parity) of the solutions. All dynamo solutions in the database have dipole-like (antisymmetric) polarity enforced by setting:.

{E5.22b}
$$\frac{\partial A(r,\pi/2)}{\partial\theta} = 0, \qquad B(r,\pi/2) = 0 \ , \qquad \text{[Antisymmetric]} \ , \tag{1.9}$$

while for symmetric (quadrupole-like) modes one would have set instead

{E5.22c}
$$A(r,\pi/2) = 0, \qquad \frac{\partial B(r,\pi/2)}{\partial\theta} = 0 \ , \qquad \text{[Symmetric]} \ . \tag{1.10}$$

{sec:ingredients}

1.2 Model ingredients

The numerical solution of eqs. (1.4)–(1.5) requires the specification of various functionals defining the inductive flows as well as source and dissipative terms. These are described in this section. In all cases we opt to use simple analytical parameterizations, either calibrated on observations, extracted from numerical simulations, and/or motivated on physical ground. For the illustrative purposes of this dynamo lab, this is entirely appropriate.

1.2.1 The differential rotation {ssec:difrot}

This is Ω in eq. (1.5). Differential rotation is driven by Reynolds stresses associated with turbulent convection and is essentially unavoidable in a rotating, convecting system (see §III.5.5). For $\Omega(r,\theta)$ we use here a simple solar-like parametrization, scaled in terms of the surface equatorial rotation rate:

$$\Omega(r,\theta) = \Omega_C + \frac{\Omega_S(\theta) - \Omega_C}{2}\left[1 + \mathrm{erf}\left(\frac{r - r_c}{w}\right)\right] , \qquad (1.11) \quad \{\texttt{E5.68a}\}$$

where

$$\Omega_S(\theta) = (1 - a_2\cos^2\theta - a_4\cos^4\theta) \qquad (1.12) \quad \{\texttt{E5.68b}\}$$

with parameter values $\Omega_C = 0.939$, $a_2 = 0.1264$, $a_4 = 0.1591$, $r_c/R = 0.7$, and $w/R = 0.05$, as inferred helioseismologically (see, e.g., Kosovichev 1996, ApJL, **469**, L61; Antia et al. 1998, MNRAS, **298**, 543; Charbonneau et al. 1999, ApJ, **527**, 445). Figure 1.1 below shows the corresponding isocontours of angular velocity, together with radial cuts at the pole, equator and mid-latitudes.

It should be noted that such a solar-like differential rotation profile is quite complex from the point of view of dynamo modelling, in that it is characterized by *three* partially overlapping shear regions: a strong positive radial shear in the equatorial regions of the tachocline, an even stronger negative radial shear in its polar regions, and a significant latitudinal shear throughout the convective envelope and extending partway into the tachocline. As shown on panel B of Fig. 1.1, for a tachocline of half-thickness $w/R = 0.05$, the mid-latitude latitudinal shear at $r/R = 0.7$ is comparable in magnitude to the equatorial radial shear; its potential contribution to dynamo action should not be casually dismissed. Conspicuously missing is the so-called surface shear layer also evidenced by helioseismology; it is usually deemed of secondary importance for internal dynamo action (but see Brandenburg 2005, ApJ, **625**, 539).

1.2.2 The total magnetic diffusivity

This is η in eqs. (1.4)–(1.5). Assuming that the total magnetic diffusivity $\eta(r)$ varies only with depth, we use the same error-function radial profile as before, normalized to the turbulent diffusivity η_0 in the convective envelope:

$$\frac{\eta(r)}{\eta_0} = \Delta\eta + \frac{1 - \Delta\eta}{2}\left[1 + \mathrm{erf}\left(\frac{r - r_c}{w}\right)\right] . \qquad (1.13) \quad \{\texttt{eq:eta}\}$$

The corresponding profile is plotted on Fig. 1.1 as a dash-dotted line. In practice, the core-to-envelope diffusivity ratio $\Delta\eta \equiv \eta_c/\eta_0$ is treated as a model parameter, with of course $\Delta\eta \ll 1$, since we associate η_c with the microscopic magnetic diffusivity, and η_0 with the presumably much larger mean-field turbulent diffusivity β (see §I.3.4.3). With the microscopic diffusivity $\eta_c \sim 1\,\mathrm{m^2 s^{-1}}$ below the core-envelope interface, and taking mean-field estimates of β at face value, one obtains $\Delta\eta \sim 10^{-9}$—10^{-6}. The solutions in the database you will be using have $\Delta\eta = 10^{-3}$—10^{-1}, which is much larger, but still small enough to nicely illustrate some important consequence of radial gradients in magnetic diffusivity.

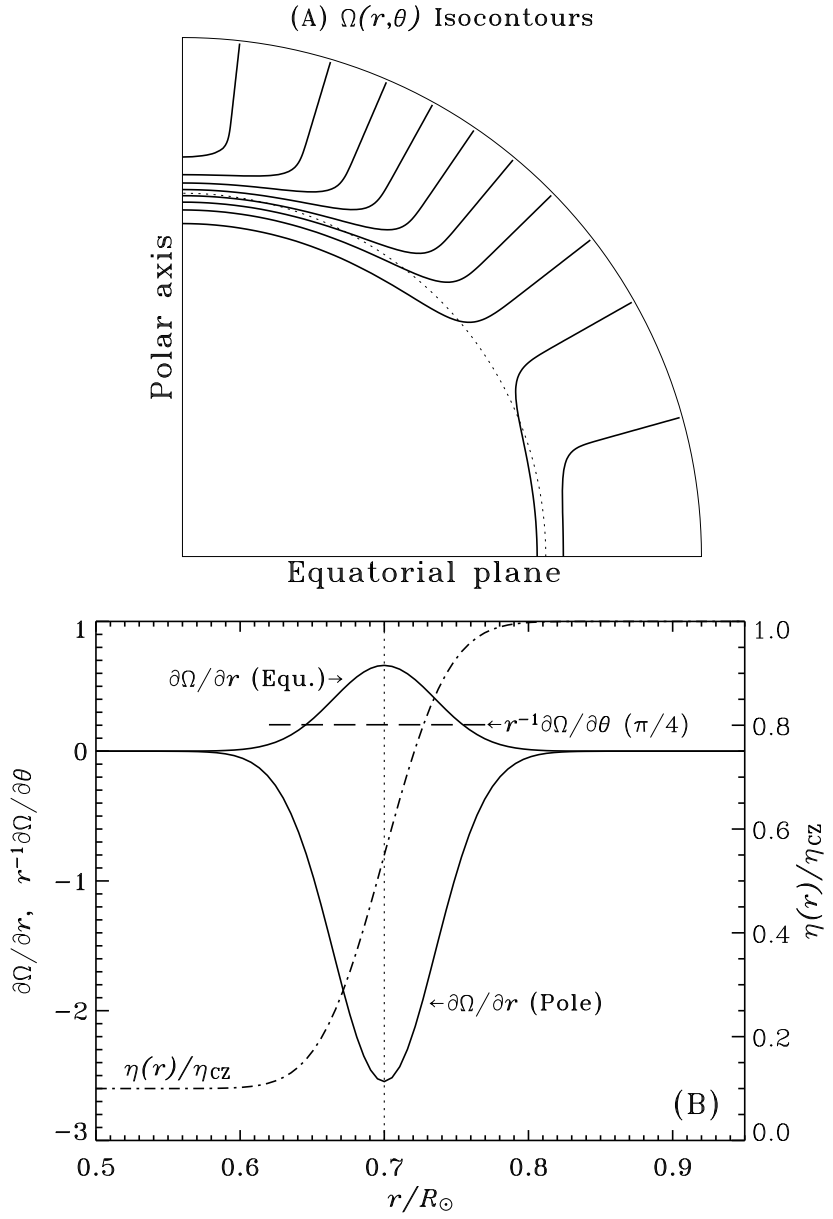

Figure 1.1: Isocontours of angular velocity generated by eqs. (1.11)—(1.12), with parameter values $w/R = 0.05$, $\Omega_C = 0.8752$, $a_2 = 0.1264$, $a_4 = 0.1591$ (panel A). The radial shear changes sign at colatitude $\theta = 55°$. Panel B shows the corresponding angular velocity gradients, together with the total magnetic diffusivity profile defined by eq. (1.13) (dash-dotted line, here with $\Delta\eta = 0.1$ for illustrative purposes). The core-envelope interface is located at $r/R = 0.7$ (dotted lines). {`fig:dr`}

1.2.3 The meridional circulation {ssec:circmed}

This is a contribution to $\mathbf{u}_p$ in eqs. (1.4)–(1.5), and denoted by $\mathbf{u}_\mathrm{M}$ in what follows. Meridional circulation is also unavoidable in turbulent rotating convective shells and results from an imbalance between Reynolds stresses and buoyancy forces (see §III.5.5). A $\sim 15\,\mathrm{m\ s^{-1}}$ poleward flow observed at the surface requires an equatorward return flow to satisfy mass conservation. Recent helioseismic measurements and analyses based on magnetic feature tracking suggest that this return flow occurs well within the convection zone, with multiple flow cells present in the convection zone (REFs), although most dynamo models to date have used a monolithic single-cell per meridional quadrant.

For all models discussed below including a meridional circulation $\mathbf{u}_\mathrm{M}(r,\theta)$, we use the following convenient parametric form, designed by van Ballegooijen & Choudhuri (1988, ApJ, **333**, 965):

$$u_r(r,\theta) = 2u_0 \left(\frac{R}{r}\right)^2 \left[-\frac{1}{m+1} + \frac{c_1}{2m+1}\xi^m - \frac{c_2}{2m+p+1}\xi^{m+p}\right]$$

$$\times\xi[(q+2)\cos^2\theta - \sin^2\theta]\sin^q\theta\ , \tag{1.14}$$ {eq:cm1}

$$u_\theta(r,\theta) = 2u_0 \left(\frac{R}{r}\right)^3 \left[-1 + c_1\xi^m - c_2\xi^{m+p}\right]\sin^{q+1}\cos\theta\ , \tag{1.15}$$ {eq:cm2}

with

$$c_1 = \frac{(2m+1)(m+p)}{(m+1)p}\xi_b^{-m}\ , \tag{1.16}$$ {eq:cm3}

$$c_2 = \frac{(2m+p+1)m}{(m+1)p}\xi_b^{-(m+p)}\ , \tag{1.17}$$ {eq:cm4}

$$\xi = \frac{R}{r} - 1\ , \tag{1.18}$$ {eq:cm5}

$$\xi_b = \frac{R}{r_b} - 1\ . \tag{1.19}$$ {eq:cm6}

Don't get too jazzed by the intricate look of these expressions, and the large number of constants they introduce. This formulation allows the generation of a wide class of meridional flows, all satisfying the mass conservation ($\nabla\cdot(\rho\mathbf{u}_p) = 0$) for a polytropic density profile of the form:

$$\frac{\rho(r)}{\rho_b} = \left(\frac{R}{r} - 1\right)^m\ . \tag{1.20}$$ {eq:cm7}

Setting $m = 0.5$, $p = 0.25$ and $q = 0$, this defines a steady quadrupolar circulation pattern, with a single flow cell per quadrant extending from the surface down to a depth r_b. Circulation streamlines are shown on Fig. 1.2, together with radial cuts of the latitudinal component at mid-latitudes ($\theta = \pi/4$), here for $r_b/R = 0.675$. The flow is poleward in the outer convection zone, with an equatorward return flow peaking slightly above the core-envelope interface, and rapidly vanishing below.

In the solution database, the only parameters that are varied are the mid-latitude surface flow speed u_0, and the lower extent r_b of the equatorward return flow.

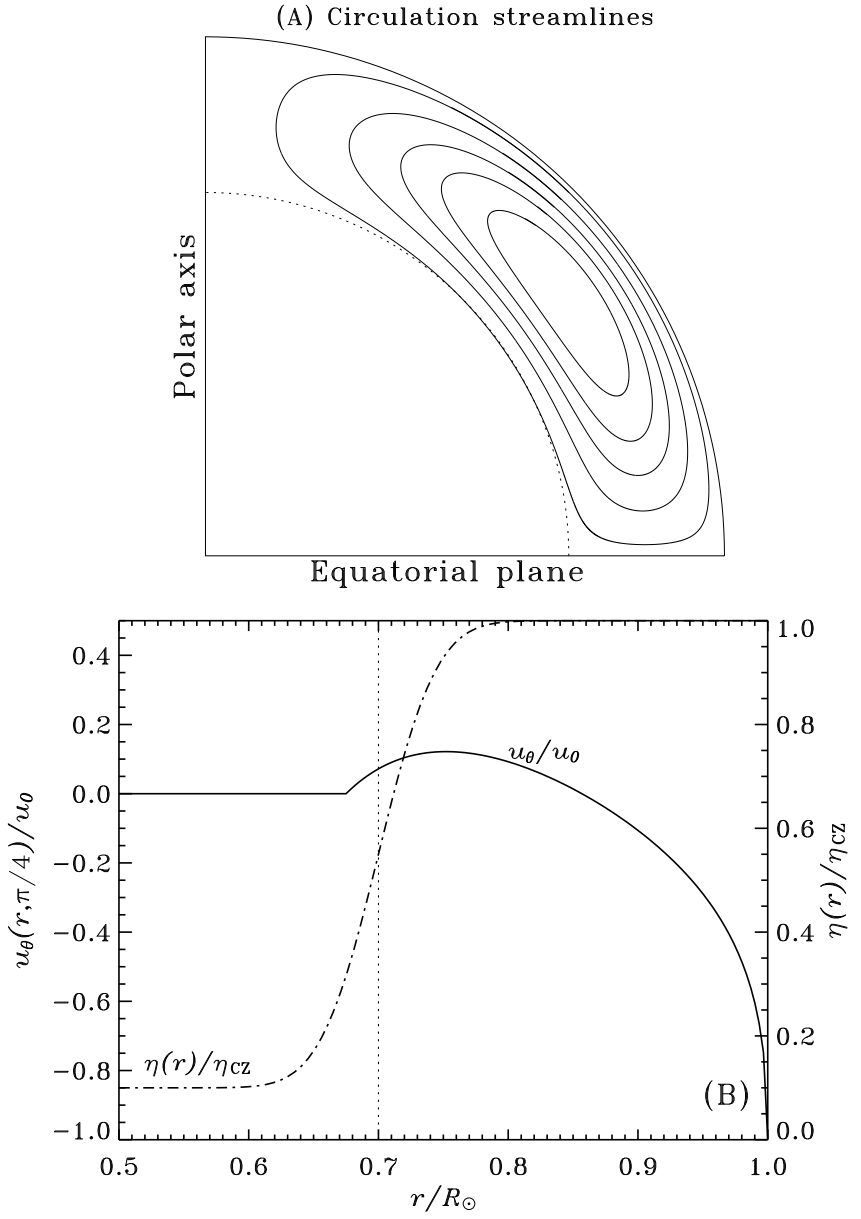

Figure 1.2: Streamlines of meridional circulation (panel A), together with the total magnetic diffusivity profile defined by eq. (1.13) (dash-dotted line, again with $\Delta\eta = 0.1$) and a mid-latitude radial cut of u_θ (bottom panel). The dotted line is the core-envelope interface. This is the analytic flow defined by eqs. (1.14)–(1.19), with parameter values $m = 0.5$, $p = 0.25$, $q = 0$ and $r_b = 0.675$. {fig:cm}

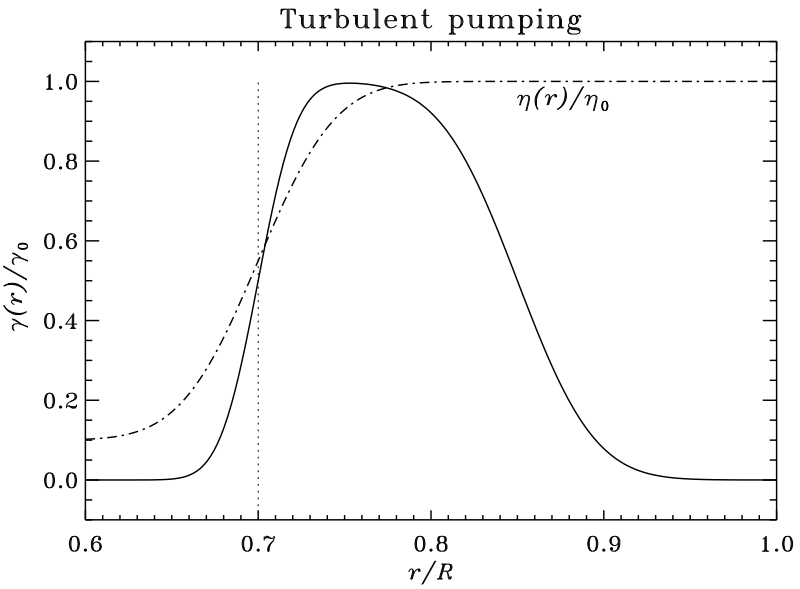

Figure 1.3: Radial profile of the turbulent pumping speed for all models in the solution database for which this physical effect is incorporated. Both the r- and θ-component of the turbulent pumping velocity share this profile, as defined by eq. (1.23) with parameter values $r_c = 0.7$, $d_1 = 0.025$, $r_2 = 0.85$, and $d_2 = 0.05$. The total magnetic diffusivity profile is shown as a dash-dotted line. The core-envelope interface is located at $r/R_\odot = 0.7$ (vertical dotted line). {fig:turbpump}

1.2.4 Turbulent pumping {ssec:turbpump}

This is another contribution to $\mathbf{u}_p$ in eqs. (1.4)–(1.5), denoted by $\boldsymbol{\gamma}$ in what follows. Turbulent pumping is a pseudo-flow, in the sense that it is an advective contribution to the turbulent electromotive force in mean-field theory and so affects only the large-scale magnetic field (§I.3.4.3); a drop of ink dropped in the sun would not feel turbulent pumping!

The parameterization used here is inspired by measurements of turbulent pumping in MHD numerical simulations of solar convection (see, e.g., Käpylä et al. 2006, A&A, **455**, 401; Racine et al. 2011, ApJ, **735**:46). These measurements indicate that turbulent pumping is predominantly downwards in the bulk of the convection zone, with an equatorward latitudinal component peaking at low latitudes. Here we model this through:

$$\gamma_r(r) = -\gamma_0 f(r) \ , \tag{1.21}$$ {eq:gamr}

$$\gamma_\theta(r,\theta) = \gamma_0 f(r) \sin^2\theta \cos\theta \tag{1.22}$$ {eq:gamth}

where

$$f(r) = \frac{1}{4}\left[1 + \mathrm{erf}\left(\frac{r-r_c}{d_1}\right)\right]\left[1 - \mathrm{erf}\left(\frac{r-r_2}{d_2}\right)\right] \ . \tag{1.23}$$ {eq:gamfr}

with $d_1 = 0.025$, $r_2 = 0.85$, and $d_2 = 0.05$. The resulting radial profile $f(r)$ is plotted on Fig. 1.3. The quantity γ_0 [m s^{-1}] measures the strength of turbulent pumping; this is the only parameter that is varied in the solution database, so that the ratio γ_r/γ_θ remains the same as γ_0 changes.

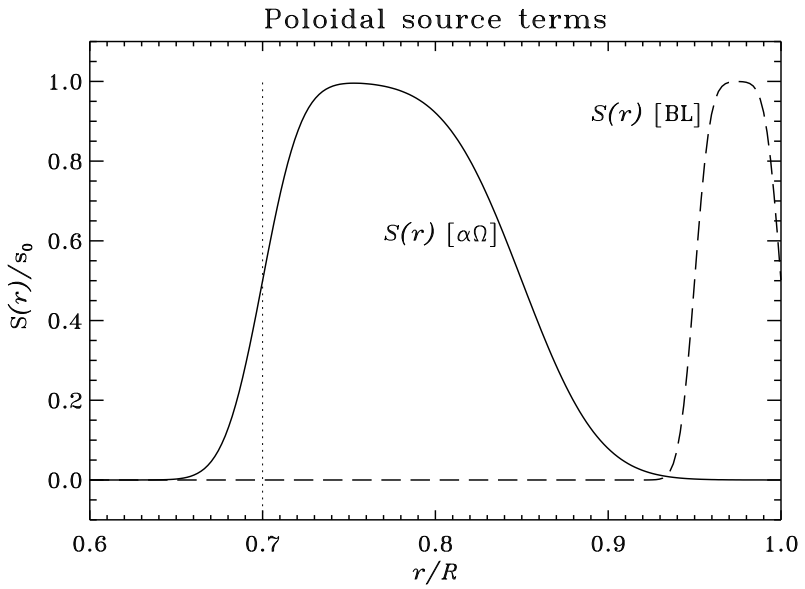

Figure 1.4: Radial profiles of the poloidal source terms for the $\alpha\Omega$ mean-field model (solid line), as defined by by eqs. (1.24)—(1.25), with parameter values $r_c = 0.7$, $d_1 = 0.025$, $r_3 = 0.85$, and $d_3 = 0.05$. The dashed line shows the radial profile for the Babcock-Leighton source term, as defined by by eqs. (1.26)—(1.27), with parameter values $r_4 = 0.95$, $d_4 = 0.01$, $r_5 = 1.0$, and $d_5 = 0.01$. The core-envelope interface is located at $r/R_\odot = 0.7$ (vertical dotted line). {fig:sourceterms}

1.2.5 Poloidal source terms {ssec:source}

This is S in eq. (1.4). Dynamo solutions for two classes of source terms are used in the solution database. The first is the classical local α-effect of mean-field electrodynamics (§I.3.4):

$$S(r,\theta;B) = \alpha(r,\theta)B(r,\theta,t) \ , \qquad [\alpha\Omega] \tag{1.24}$$ {eq:saO}

where

{eq:saOfr}
$$\alpha(r,\theta) = \frac{s_0}{4}\left[1+\mathrm{erf}\left(\frac{r-r_c}{d_1}\right)\right]\left[1-\mathrm{erf}\left(\frac{r-r_2}{d_2}\right)\right]\cos(\theta) \ . \tag{1.25}$$

with parameter values $r_3 = 0.85$ and $d_2 = 0.05$, so that the radial dependency is the same as for the turbulent pumping speed $\boldsymbol{\gamma}$, reflecting the fact that the α-effect and turbulent pumping both from the same turbulent electromotive force. The combination of error functions concentrates the α-effect in the bottom half of the envelope, and let it vanish smoothly below, just as the net magnetic diffusivity does (i.e., we again set $r_c/R = 0.7$ and $w/R = 0.05$). The corresponding radial profile is plotted on Fig. 1.4. Various lines of argument point to an α-effect peaking in the bottom half the convective envelope, since there the convective turnover time is commensurate with the solar rotation period, a most favorable setup for the type of toroidal field twisting at the root of the α-effect. Likewise, the hemispheric dependence of the Coriolis force suggests that the α-effect should be positive in the Northern hemisphere, and change sign across the equator ($\theta = \pi/2$). The "minimal" latitudinal dependency is thus $\cos\theta$. These expectations are generally borne out by measurements of the α-tensor in MHD simualtions of solar convection (e.g., Ossendrijver et al. 2001, A&A, **376**, 713; Racine et al. 2011, ApJ, **735**:46; and refereces therein)

For dynamo models relying on the Babcock-Leighton mechanism of poloidal field regeneration, the source term S to be inserted in eq. (1.4) is given instead by:

{eq:sBL}
$$S(r,\theta,B(t)) = s_0\, f(r) \sin\theta\cos\theta B(r_c,\theta,t) \ , \qquad [\text{Babcock} - \text{Leighton}] \tag{1.26}$$

where

{eq:sBLfr}
$$f(r) = \frac{1}{4}\left[1+\text{erf}\left(\frac{r-r_4}{d_4}\right)\right]\left[1-\text{erf}\left(\frac{r-r_5}{d_5}\right)\right] \ , \tag{1.27}$$

where s_0 is a numerical coefficient setting the strength of the source term, and with the various remaining numerical coefficient taking the values $r_4 = 0.95$, $r_5 = 1$, $d_4 = d_5 = 0.01$. Note that the dependency on B is *non-local*, i.e., it involves the toroidal field evaluated at the core-envelope interface r_c, (but at the same polar angle θ). The combination of error functions concentrates the source term immediately beneath the surface, which is where the Babcock-Leighton mechanism is observed to operate. The $\sin\theta\cos\theta$ dependency is a first order description of Joy's Law, i.e., the tilt of active regions increases with latitude at low latitudes, but the tilts become randomized by convection for weakly magnetized flux ropes emerging at high latitudes. The nonlocality in B represents the fact that the strength of the source term is proportional to the field strength in the bipolar active region, itself presumably reflecting the strength of the diffuse toroidal field near the core-envelope interface, where the magnetic flux ropes eventually giving rise to the bipolar active region presumably originate.

This specific formulation of the Babcock-Leighton source term is taken directly from Dikpati & Charbonneau (1999, ApJ, **518**, 508), and ha the practical advantage of being readily incorporated in the classical mean-field dynamo equations. A number of alternate but conceptually equivalent formulations do exist in the literature (e.g., Nandy & Choudhuri 2001, ApJ, **551**, 576; Munoz-Jaramillo et al. 2010, ApJ, **720**, L20; Yeates & Munoz-Jaramillo 2013, MNRAS, **436**, 3366).

Whether working with $\alpha\Omega$ or Babcock-Leighton models, all spatial dependencies are held fixed, with parameter values as specified above. The parameter s_0 measuring the overall magnitude of the poloidal source term is the only source-term-related parameter varying for all dynamo solutions in the database.

1.2.6 The amplitude-quenching nonlinearity {ssec:quenching}

With the flow and source terms time-independent and specified a priori, eqs. (1.4)–(1.5) are linear in A and B and will accept eigensolutions $\propto \exp(st)$, with s a (complex) eigenvalue. For dynamo solutions, $\text{Re}(s) > 0$ and unbounded exponential growth will ensue. To bypass this problem we introduce the simplest amplitude-limiting nonlinearity of common usage in solar/stellar dynamo modelling, namely the so-called "α-quenching". This consists in multiplying the source term amplitude parameter s_0 by a toroidal field-dependent prefactor which tends to zero as the field strength exceeds an equilibrium value B_{eq}.

{???}
$$s_0 \to \frac{s_0}{1+(B(r,\theta,t)/B_{\text{eq}})^2} \ , \tag{1.28}$$

where the equilibrium field strength B_{eq} then setting the absolute scale of the magnetic field amplitude. All solutions in the database use $B_{\text{eq}} = 0.5\,\text{T}$. Note that for the Babcock-Leighton source term, the toroidal field B on the RHS of this expression is evaluated at the core-envelope interface r_c rather than locally at r, in keeping ith the non-local nature of this poloidal source mechanism.

Notably missing in the Babcock-Leighton context is a lower toroidal field threshold on S, to mimic the fact that flux ropes with field strengths lower than a few teslas either fail to be destabilized in a short enough timescale, rise to the surface at high latitudes and without systematic tilt patterns, and/or fail altogether to survive their rise through the convective

envelope. Including such a lower threshold has interesting consequences for the behavior of the resulting dynamo model (see, e.g., Charbonneau et al. 2005, ApJ, **619**, 613), but things being complicated enough as is, for this lab we'll just stick to the same algebraic amplitude-quenching nonlinearity for both classes of source terms.

Physically, the quenching nonlinearity intoduced in $\alpha\Omega$ models captures the fact that a stronger toroidal field is harder for cyclonic convection to twist and give rise to an α-effect (see §I.3.5.2 and III.6.2.1.2). In the Babcock-Leighton context, the nonlocal quenching nonlinearity reflects the fact that as the strength of the flux rope reaches about 2 T, it emerges without the East-West tilt essential to the Babcock-Leighton mechanism. (see §III.6.2.2).

{ssec:scaling}

1.3 Scalings, dynamo numbers and Reynolds numbers

With all "ingredients" specified, our next step is to put the dynamo equations into nondimensional form. This can actually be carried out in a number of ways. We opt here to scale all lengths in terms of the star's radius R, and time in terms of the corresponding diffusion time $\tau = R^2/\eta_0$. Equations (1.4)–(1.5) become

{E5.16a}

$$\frac{\partial A}{\partial t} = \left(\nabla^2 - \frac{1}{\varpi^2}\right) A - \frac{1}{\varpi}(\mathrm{R}_M \mathbf{u}_M + \mathrm{R}_T \boldsymbol{\gamma}) \cdot \nabla(\varpi A) + C_\alpha S \tag{1.29}$$

$$\frac{\partial B}{\partial t} = \left(\nabla^2 - \frac{1}{\varpi^2}\right) B \frac{1}{\varpi}\frac{\partial(\varpi B)}{\partial r}\frac{\partial \eta}{\partial r} - \varpi \nabla \cdot \left(\frac{B}{\varpi}(\mathrm{R}_M \mathbf{u}_M + \mathrm{R}_T \boldsymbol{\gamma})\right)$$

{E5.16b}

$$+ C_\Omega \varpi (\nabla \times A) \cdot (\nabla \Omega) \ , \tag{1.30}$$

where we have also explicitly separated the total poloidal flow $\mathbf{u}_p$ of eqs. (1.4)–(1.5) into its contributions arising from meridional circulation ($\mathbf{u}_M$, §1.2.3) and turbulent pumping ($\boldsymbol{\gamma}$, §1.2.4). The scaling procedure has led to the appearance of four nondimensional numbers:

{E5.17a}

$$C_\alpha = \frac{s_0 R}{\eta_0} \ , \tag{1.31}$$

{E5.17b}

$$C_\Omega = \frac{\Omega_0 R^2}{\eta_0} \ , \tag{1.32}$$

{E5.17c}

$$\mathrm{R}_M = \frac{u_0 R}{\eta_0} \ , \tag{1.33}$$

{E5.17d}

$$\mathrm{R}_T = \frac{\gamma_0 R}{\eta_0} \ , \tag{1.34}$$

with s_0 (dimension m s^{-1}), η_0 (dimension m^2 s^{-1}), u_0 (dimension m s^{-1}) γ_0 (dimension m s^{-1}) and Ω_0 (dimension s^{-1}) as reference values for the poloidal source, diffusivity, surface meridional flow, turbulent pumping speed, and shear, respectively. Remember that the functionals S, η, $\mathbf{u}_M$, $\boldsymbol{\gamma}$ and Ω are hereafter dimensionless quantities. The quantities C_α and C_Ω are **dynamo numbers**, measuring the importance of inductive versus diffusive effects on the RHS of eqs. (1.29)–(1.30). The other two dimensionless numbers, R_M and R_T, are Reynolds numbers, measuring the relative importance of advection (by meridional circulation for R_M, and by turbulent pumping for R_T) versus diffusion (by Ohmic dissipation) in the transport of A and B in meridional planes.

These four dimensionless parameters are the primary "knobs" with are varied when building dynamo models applicable to the sun and stars, so let's get some numerical estimates for their values. The turbulent diffusivity at the base of the solar convective envelope is estimated to be

{???} $$\eta_0 = 5 \times 10^7 \,\mathrm{m}^2\,\mathrm{s}^{-1} \ , \tag{1.35}$$

which yields a diffusion time:

{???} $$\tau = \frac{R^2}{\eta_0} = 10^{10}\,\mathrm{s} \simeq 300\,\mathrm{yr} \ . \tag{1.36}$$

For the sun,

$$\Omega_{\rm eq} = 2.6 \times 10^{-6}\,\mathrm{rad}^2\,\mathrm{s}^{-1} \ , \tag{1.37}$$ {???}

so that

$$C_\Omega = 2.6 \times 10^4 \ , \tag{1.38}$$ {???}

With a surface meridional flow speed $u_0 \sim 15\,\mathrm{m\ s}^{-1}$,

$$\mathrm{R}_M \simeq 200 \ , \tag{1.39}$$ {???}

while of the turbulent pumping speed extracted from numerical simulations suggest $\gamma_0 \sim 1\,\mathrm{m\ s}^{-1}$, so that

$$\mathrm{R}_T \simeq 15 \ . \tag{1.40}$$ {???}

Estimates for the source term amplitude of either the α-effect of $\alpha\Omega$ mean-field models, or of the Babcock-Leighton mechanism, are the most ill-constrained observationally. Values of a few m s^{-1} are often used, leading to C_α in the range 5–50.

1.4 Numerical implementation {sec:numerics}

Algorithmic details regarding how eqs. (1.29)–(1.30) are solved numerically matter little for this lab, but for those interested in such matters, what follows is a brief synopsis.

The solution domain is the N-hemisphere meridional plane, on which a 2D cartesian grid in $[r, \cos(\theta)]$ is defined. The dynamo equations are discretized on this grid using bilinear Galerkin finite elements. Although computationally heavier than finite differences, the use of finite elements has a number of practical advantages, most notably here the fact that the discretization error is not affected by the definition of a mesh where cells vary in size across the domain. This is important here because of the sharp gradients often building up in the vicinity of the core-envelope interface. The solutions included in the database are all computed on a (relatively) small grid of 96×64 in radius$\times$ latitude, as plotted on Figure 1.5.

Time stepping achieved through the implicit single-step Θ-method. Such an implicit scheme allows the use of relatively large time steps, making it possible to cover many cycles in a reasonably small number of time step, typically $\sim 10^3$. The overall code structure follows fairly closely that described in Burnett (1988, *Finite Element Analysis*, Reading:Addison-Wesley).

The initial condition is a weak global toroidal field, and the dynamo equations are integrated until the solutions has reached a statistically stationary state. At every time step, the poloidal vector potential and toroidal field values at every mesh node are written to file.

1.5 The solution database {sec:database}

The various tasks associated with the Lab (as detailed in §1.7 below) basically involve running $\alpha\Omega$ or Babcock-Leighton dynamo models, varying a subset of the defining parameters C_α,

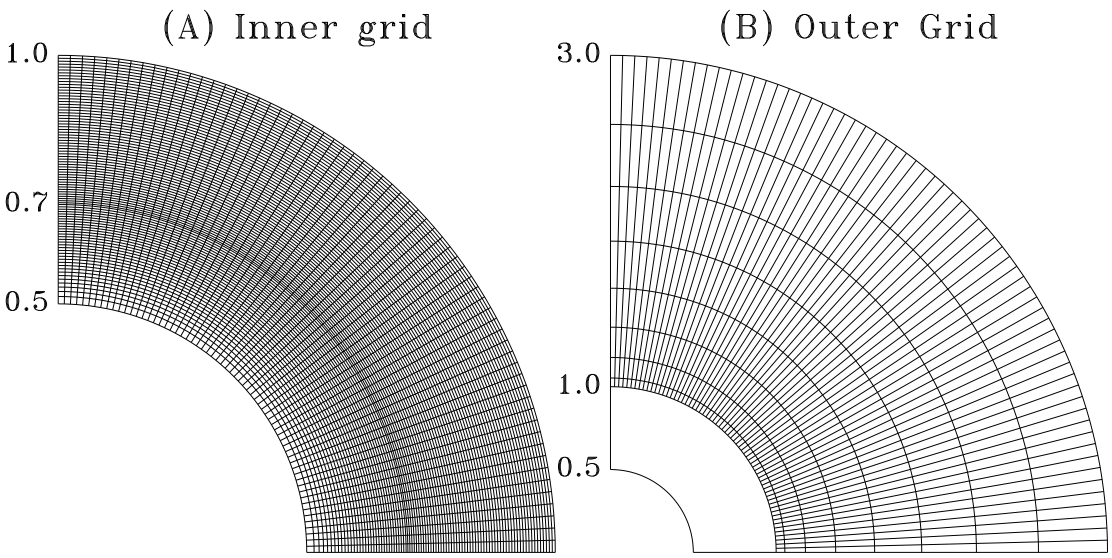

Figure 1.5: The computational grid in physical space. Part (A) shows the grid within the star's meridional quadrant, with the thick line indicating the core-envlope interface $r_c/R = 0.7$ for a "solar" model. Part (B) indicates the outer computational grid tiling the "buffer zone" within which the zero-current eqs. (1.7)–(1.8) are simultaneously solved. On each panel, the rotation (symmetry) axis runs vertically at left, and the equatorial plane horizontally at bottom. The grid shown here has dimension $N_r \times N_\theta = 96 \times 64$, which is used in all dynamo solutions included in the database. The computation itself is carried out on a cartesian grid in $[r/R, \cos\theta]$ space, with each cell tiled with a bilinear finite element. {`fig:grid`}

C_Ω, R_M, R_T, r_c, and/or r_b, and investigating the consequences of these variations on global properties of the dynamo, with an eye towards interpreting the multiplicity of magnetic activity behavior observed in late-type stars. This being a HUGE undertaking, the first decision made was to focus on dynamo activity in main-sequence solar-type stars, i.e., stars with a radiative core overlaid by a convective envelope of significant thickness.

After much consideration, and in view of the limited time available to do this lab, it was decided to assemble a database of pre-calculated dynamo solutions, and let you mine that database as a means to explore the behavior of different classes of such models in the broader context of stellar dynamos. Each solution file in the database has a name codified in such a manner as to ease the identification of the subset of solution files required to carry out the lab tasks defined in §1.7 below. Appendix A provides a list of all dynamo solutions included in ther database, each identified by this filename. Here is an example of a file name:

{`eq:filename`}

$$\underbrace{\texttt{A0}}_{1} - \underbrace{\texttt{025}}_{2} - \underbrace{\texttt{005}}_{3} - \underbrace{\texttt{200}}_{4} - \underbrace{\texttt{000}}_{5} - \underbrace{\texttt{700}}_{6} - \underbrace{\texttt{675}}_{7} \tag{1.41}$$

The various 2- or 3-digit character or integer substrings of the filename correspond to the following, as numbered in the above:

1. A two-letter code indicating which type of dynamo this is; AO= a mean-field $\alpha\Omega$ dynamo, with a local poloidal source term given by eq. (1.24); BL= a Babcock-Leighton model, with a non-local surface source term given by eq. (1.26).
2. The value of the dimensionless dynamo number C_Ω, in units of 10^3; this is a measure of the strength of differential rotation.
3. The value of the dimensionless dynamo number C_α; this is a measure of the strength of the source term.

4. The value of the dimensionless Reynolds number R_M; this is effectively a measure of the surface poleward meridional flow speed.

5. The value of the dimensionless Reynolds number R_T; this is effectively a measure of the strength of turbulent pumping.

6. The radius r_c setting base of the convecting layers, in units of 10^{-3}. of the star's radius

7. The radius r_b setting the depth of the equatorward return meridional flow, in units of 10^{-3} of the star's radius.

Therefore, the file name given above contains a $\alpha\Omega$ dynamo solution computed with $C_\Omega = 2.5 \times 10^4$, $C_\alpha = 5$, $\mathrm{R}_M = 200$, $\mathrm{R}_T = 0$, with the base o the convection zone at $r/R = 0.7$ and the meridional return flow closing at $r/R = 0.675$.

The "`.i3e`" suffix flags this file as unformatted fortran-IEEE data. Don't try to view the file's content with a text editor, it will just look like junk. The IDL analysis routine provided to analyze the solutions (see below) is set up to properly read it. The advantages of storing the solutions as unformatted data are twofold: (1) smaller filesizes in the database, and (2) swifter read-in by the IDL analysis routine.

For each solution in the database, you will find a file with the same name except for a "`.mpg`" suffix. This is a pre-computed animation of the solutions contained in each of the parent `.i3e` file, in mpeg format. Viewing these animations as you analyze the dynamo solutions will be a useful complement to the analyses carried out by the IDL analysis routine,... to which we now turn.

1.6 The IDL analysis routine {sec:idl}

Given that as a group you will be running the lab on a collection of laptop of varying speeds, ages, and operating systems, we opted to keep the bells and whitles to a minimum, and have you do the lab using a single IDL routine which is fed a filename (following the naming convection explained in the preceding section), and carries out a series of postprocessing calculations and displays results in graphical form. Normally you should not have to touch/edit anything within this IDL files, but you will need to understand what graphical and numerical information is being procuced.

Examples of the graphical output produced by the IDL software are reproduced in Figures 1.6 and 1.7 below. The information provided in these windows should allow you to carry out the task assigned to your group, as defined in §1.7 further below. Let's detail the content of each window in turn.

1.6.1 IDL Window 1

The top of IDL Window 1 first echoes the filename given as input, and writes a one-line brief description of the solution. Immediately beneath follows a list (two leftmost columns) of input parameters to the dynamo solution, following the notation established in §1.2 of these Lab Notes. The third column lists (in yellow) useful physical (dimensional) quantities associated with the solution parameters, including the envelope magnetic diffusivity η_0, the diffusion time τ in years, the surface meridional flow speed and turbulent pumping speed, both in meters per second. The fourth column lists (in purple) quantities extracted from the simulation output per se, namely (1) the peak toroidal field value at the core-envelope interface and the peak surface radial field, both in Tesla; (2) the magnetic cycle period, in years; (3) the phase lag between the toroidal field at the core-envelope interface and the surface radial field.

The first graphical panel is a time-latitude diagram of the toroidal magnetic component $B(r, \theta, t)$ extracted the depth r_c/R corresponding to the core-envelope inetrface; the equator is at bottom and the North-Pole on top, as indicated on the far left. This is usually considered the dynamo model's equivalent to the sunspot butterfly diagram. The color scale encodes the

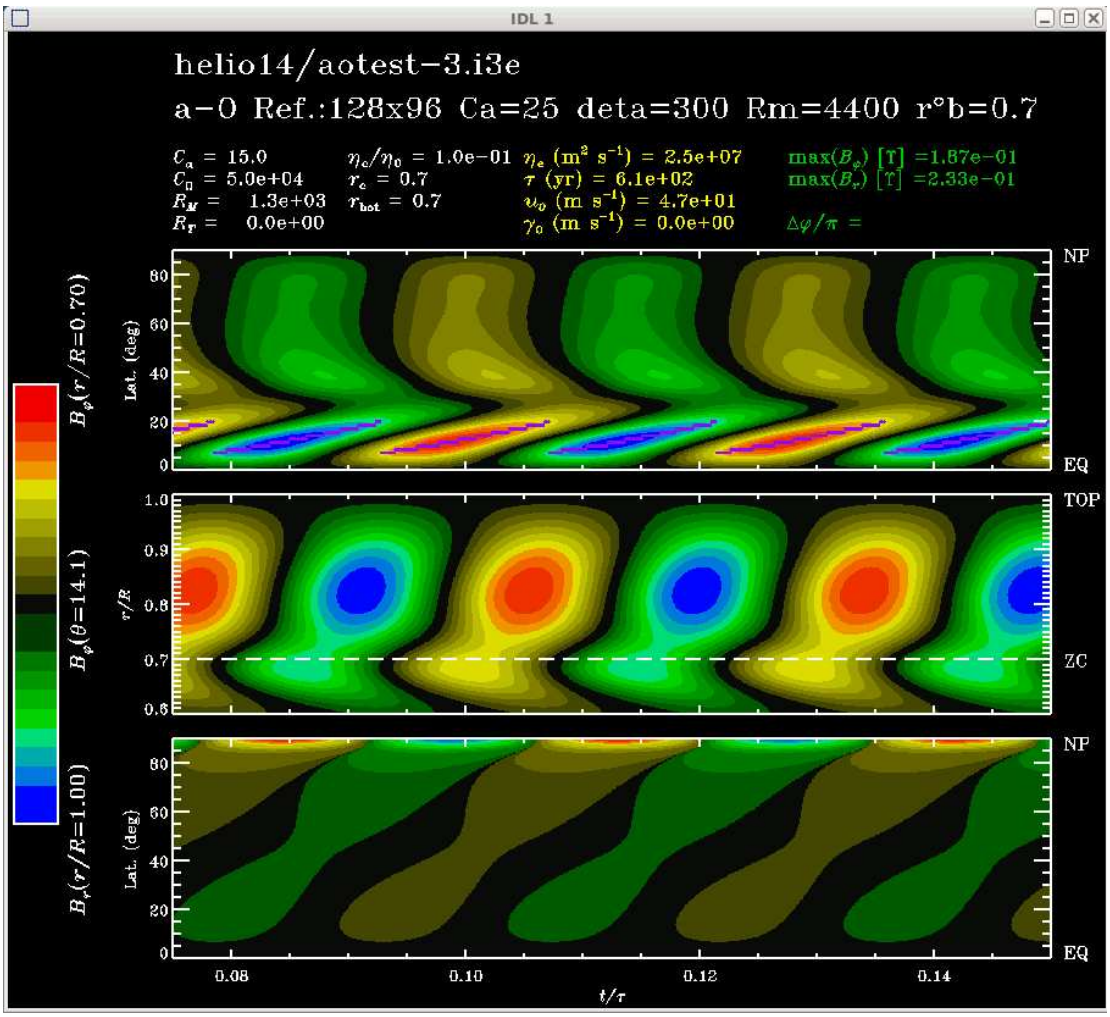

Figure 1.6: The first IDL window generated by `helio14.idl`. {`fig:IDLw1`}

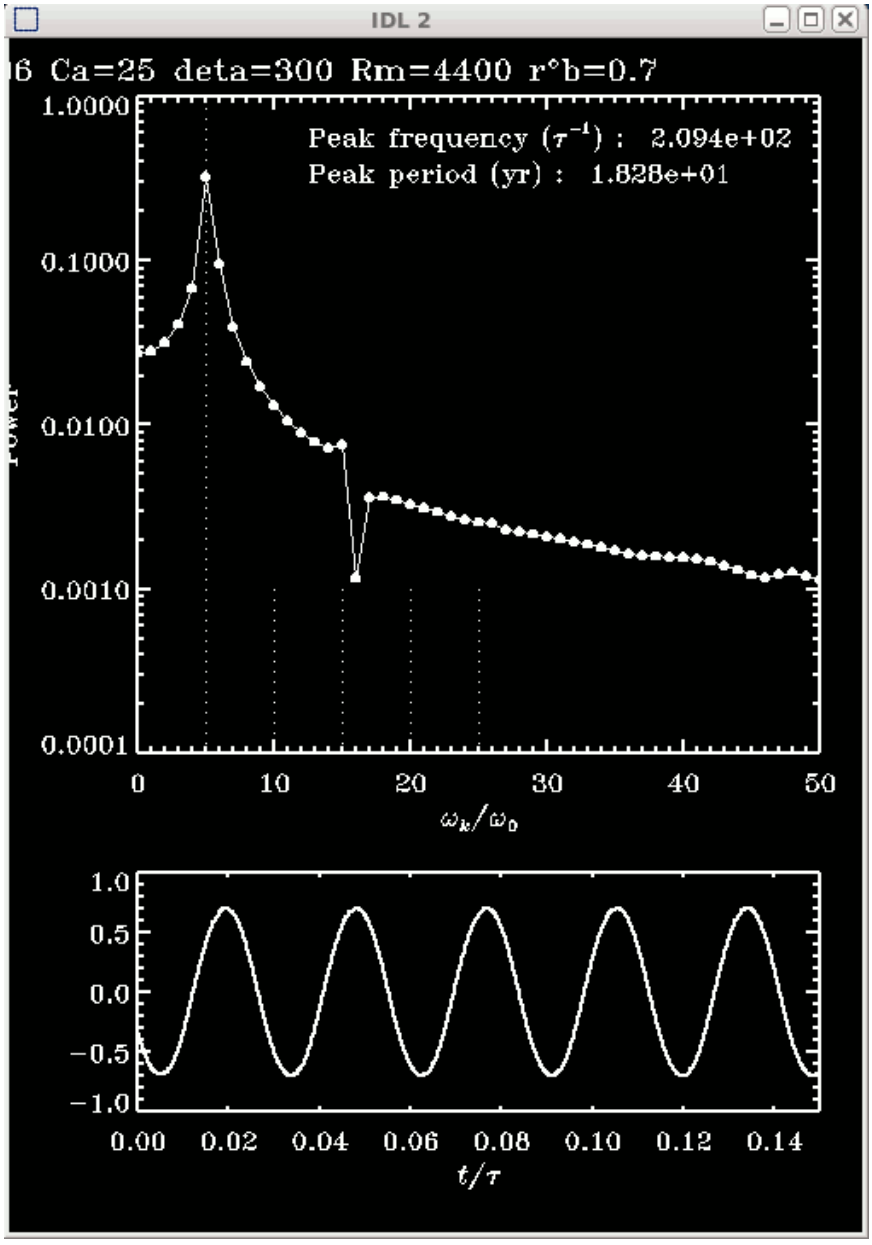

Figure 1.7: The second IDL window generated by `helio14.idl`. {`fig:IDLw2`}

field strength, normalized to the peak value listed previously. The series of purple dots indicate the latitudes of peak toroidal field at each time step within this time-latitude slice. This, presumably, would correspond to the prefered latitude for sunspot emergences. On this and the two subsequent plot, only the second half of the dynamo run is plotted, to be better able to distinguish individual cycles, and time is in units of the diffusion time τ.

The middle graphical panel is now a time-radius slice extracted at the latitude of peak toroidal field on the time-latitude slice just discussed, and normalized to the same peak field strength. The horizontal dashed line indicates the core-envelope interface r_c/R.

The bottom graphical panel is a time-latitude slice of the radial magnetic component at the surface ($r/R = 1$), normalized to the peak values given in the top-right column.

1.6.2 IDL Window 2

The second IDL window plots a time-series of the toroidal field extracted at point (r_c, θ_m) in the meridional plane, where r_c is the core-envelope interface the latitude at which the toroidal component reaches it maximal value at the peak of the cycles. The top panels shows the power spectrum of this time series, computed by Fast Fourier Tranform. Note also that the vertical scale is logarithmic.

The vertical dotted line flags the peak frequency in the spectrum, listed at top right of the plot along with the cycle period The shorter dotted vertical line segments indicate the first 5 harmonics of the primary peak, which may or may not show significant power, according to the degree to which the underlying time series departs from sinusoidal shape.

1.6.3 Example IDL session

You will be given access to an IDL source file, named `helio14.idl`. The file containes a number of IDL procedures which must be compiled prior to running the main viewing procedure `viewdynamo`; this procedure must be called with three arguments:

1. A valid filename pointing to a file in the database; PLEASE NOTE: the file name must be typed inside quotes, so IDL can identify it as a character string;

2. A fractional radius at which the top time-latitude diagram of the toroidal field is constructed (see Fig. 1.6), the valid range being $[0.5, 1.0]$; if you enter a value outside of this range, a default value equal to the base of the convection zone r_c/R is used;

3. A latitude in degrees at which the middle time-radius diagram of the toroidal field is constructed (see Fig. 1.6), the valid range being $[0, 90]$; if you enter a value outside of this range, a default value of 45° is used.

Figure 1.8 shows how to go about starting a typical analysis, with IDL launched from a "terminal" window. The steps are, line by line:

1. Launch IDL by imply typing `idl` <return> at the command line;

2. compile the IDL procedures by typing `.run helio14.idl` <return>

3. view the solution by calling the `viewdynamo` procedure contained in the `helio14.idl` source file. In the specific example shown in Fig. 1.8, the time-latitude diagram is extracted at the default value $r_c = 0.7$ and the time-radius diagram at $\theta = 60°$, for an $\alpha\Omega$ dynamo solution with parameter values $C_\alpha = 10$, $C_\Omega = 5 \times 10^4$, $\mathrm{R}_M = 100$, $\mathrm{R}_T = 0$, $r_c/R = 0.7$, and $r_b = 0.675$.

As your first validation test, you should try to replicate exactly the above steps, and if all goes well (!) the two windows reproduced on Figs. 1.6 and 1.7 should pop up on your screen.

Figure 1.8: Screenshot of a typical dynamo analysis session; here the file analyzed is called `AO-050-010-100-000-700-675.i3e`, the default value $r_c = 0.7$ is used for the depth at which the toroidal field time-latitude diagram is constructed, and the time-radius diagram is extracted at latitude of 60°. This session produced the two windows reproduced on Figs. 1.6 and 1.7. {`fig:IDLcmd`}

{sec:tasks}

1.7 The tasks

You are finally ready to get to work.

Here is a (non-exhaustive) list of quantities whose variations may be interesting to track as you work through your sequence of dynamo solutions:

1. The cycle period;
2. The ratio of surface poloidal to deep toroidal field; even though thre absolute scale of the magnetic field is set by our adopted algebraic α-quenching nonlinearity, this ratio remains a meaningful quantity.
3. The occurence of multiple dynamo modes, and/or long-timecale modulations of the dynamo solution. Both can arise through "interference" between dynamo modes feeding on distinct source regions, and do materialize in some corners of the parameter space for this dynamo model;
4. The concentration of the magnetic field at or beneath the core-envelope interface;
5. The concentration of the surface magnetic field at polar latitudes;
6. The phase lag between the surface and deep magnetic field;

1.7.1 Impact of meridional flows in $\alpha\Omega$ dynamo solutions

vary meridional flow speed, depth of return flow, dynamo number

Here are a few specific queries and suggestions, to get you going:

1. Starting with the $\mathrm{R}_M = 0$ solution, why is the dynamo mode confined to relatively high latitudes here, and why is the mode propagating equatorward ?
2. What happens to the dynamo period as the meridional flow speed increases (via increasing R_M)?
3. Do you perceive a transition in the mode of dynamo action, as R_M is increased ? Is this transition abrupt of gradual ?

If lacking inspiration, see §III.6.X in your *Heliophysics* textbooks.

1.7.2 Impact of meridional flows in Babcock-Leighton dynamo solutions

vary meridional flow speed, depth of return flow, dynamo number

If lacking inspiration, see Dikpati & Charbonneau (1999, ApJ, **XXX**, YYY).

1.7.3 Impact of turbulent pumping in Babcock-Leighton models with shallow meridional flows

vary depth of meridional flow and turbulent pumping speed

If lacking inspiration, see Guerrero & Gouveia Dal Pino (2008, A&A, **485**, 267).

1.7.4 Impact of rotation rate on $\alpha\Omega$ dynamo solutions

Try out various prescriptions on how model ingredients reacts to change in rotation rate Vary first just C_α; then C_α and C_Ω; then C_α, C_Ω and R_M.

If lacking inspiration, see §III.6.X in your *Heliophysics* textbooks.

1.7.5 Impact of deepening convection zone on $\alpha\Omega$ dynamo solutions

Try out various prescriptions on how model ingredients reacts to change in depth of convection zonei (i.e., decreasing luminosity).

First vary only r_c; then vary also C_α and C_Ω following reasonable prescriptions.

1.7.6 Impact of deepening convection zone on Babcock-Leighton dynamo solutions

---

Problems:

1. Obtain equations (1.4) and (1.5) by substitution of eqs. (1.2) and (1.3) into the MHD induction equation (1.1). Hint: the induction equation is a vector equation; terms "oriented" in the ϕ-direction must cancel one another independently of terms oriented perpendicular to the ϕ-direction.

2. Let's consider a constant-density "sun" made of purely ionized Hydrogen. Suppose now that its *exterior magnetic* field can be approximated by a dipole, with a surface field strength of 10^{-3} T. Assume now that this magnetic field is produced by an azimuthal (i.e., ϕ-directed) current density within the interior ($r/R_\odot < 1$); then,

   (a) Estimate the magnitude of the current density required to produce such a dipolar field;

   (b) Estimate the drift velocity between protons and electrons required to produce such a current density. How does it compare to the average thermal velocity?

   (c) How can such a small velocity difference not be erased by collisions between microscopic constituents? To answer this one will have to think back to some fundamental aspects of the induction process, as covered in your first course on electromagnetism.

3. Consider the case of shearing of a pure dipole by the parametrized solar-like differential rotation of §1.2.1 herein;

   (a) Starting from a poloidal field strength of 10^{-4} T at the core-envelope interface, calculate/estimate the time taken for the toroidal field strength to reach a strength of 1 T;

   (b) By judicious dimensional analysis of the ϕ-component of the inviscid form of of the momentum equation, evaluate the timescale over which the rotational shear at the core-envelope interface would be altered by the Lorentz force, once the toroidal field strength has reached 1T;

   (c) Is your result in (b) much longer or shorter than the solar cycle period? What does this suggest?

Bibliography:

If you need a refresher on undergraduate electromagnetism, you should go back to

Griffith, D.J., *Introduction to Electrodynamics*, 3rd ed., Prentice Hall (1999).

At the graduate level, the standard reference remains

Jackson, J.D., *Classical Electrodynamics*, 2nd ed., John Wiley & Sons (1975),

who does devote a chapter to magnetohydrodynamics, including a discussion of magnetic wave modes. My personal favorite on magnetohydrodynamics is:

Davidson, P.A., *An Introduction to Magnetohydrodynamics*, Cambridge University Press (2001).

Further specializing to the dynamo problem, the all-time classic is:

Moffatt, H.K. 1978, *Magnetic Field Generation in Electrically Conducting Fluids*, (Cambridge: Cambridge Univ. Press).

For more on dynamo models for the sun (and, by extension, solar-type stars), see the following recent review paper and monograph authored by yours very truly:

Charbonneau, P., 2010, LRSP, **7**,
`http://solarphysics.livingreviews.org/Articles/lrsp-2010-3/`

Appendix A

The dynamo solution database {app:database}

Table 1
The database of dynamo solutions

File Name	Model type	C_α	C_Ω	R_M	R_T	r_c	r_b
AO-010-050-000-000-700-675.i3e	$\alpha\Omega$	10	5×10^4	0	0	0.7	0.675
AO-010-050-030-000-700-675.i3e	$\alpha\Omega$	10	5×10^4	30	0	0.7	0.675
AO-010-050-050-000-700-675.i3e	$\alpha\Omega$	10	5×10^4	50	0	0.7	0.675
AO-010-050-100-000-700-675.i3e	$\alpha\Omega$	10	5×10^4	100	0	0.7	0.675
AO-010-050-200-000-700-675.i3e	$\alpha\Omega$	10	5×10^4	200	0	0.7	0.675
AO-010-050-500-000-700-675.i3e	$\alpha\Omega$	10	5×10^4	200	0	0.7	0.675
AO-010-050-200-000-700-675.i3e	$\alpha\Omega$	10	5×10^4	200	0	0.7	0.75
AO-010-050-200-000-700-675.i3e	$\alpha\Omega$	10	5×10^4	200	0	0.7	0.85
AO-010-050-500-000-700-675.i3e	$\alpha\Omega$	10	5×10^4	200	0	0.7	0.75
AO-010-050-500-000-700-675.i3e	$\alpha\Omega$	10	5×10^4	200	0	0.7	0.85
AO-010-050-000-000-700-675.i3e	$\alpha\Omega$	10	5×10^4	0	0	0.6	0.575
AO-010-050-000-000-700-675.i3e	$\alpha\Omega$	10	5×10^4	0	0	0.8	0.775
AO-010-050-000-000-700-675.i3e	$\alpha\Omega$	10	5×10^4	0	0	0.9	0.875